

## Original article

## Features of endogenous cardiomyocyte chromatin revealed by super-resolution STED microscopy

Scherise Mitchell-Jordan<sup>a</sup>, Haodong Chen<sup>a</sup>, Sarah Franklin<sup>a</sup>, Enrico Stefani<sup>a,c</sup>,  
Laurent A. Bentolila<sup>d,e,\*</sup>, Thomas M. Vondriska<sup>a,b,c,\*</sup>

<sup>a</sup> Department of Anesthesiology, David Geffen School of Medicine, University of California, Los Angeles, USA

<sup>b</sup> Department of Medicine, David Geffen School of Medicine, University of California, Los Angeles, USA

<sup>c</sup> Department of Physiology, David Geffen School of Medicine, University of California, Los Angeles, USA

<sup>d</sup> Department of Chemistry and Biochemistry, University of California, Los Angeles, USA

<sup>e</sup> California NanoSystems Institute, University of California, Los Angeles, USA

## ARTICLE INFO

## Article history:

Received 9 May 2012

Received in revised form 6 July 2012

Accepted 19 July 2012

Available online 28 July 2012

## Keywords:

Super-resolution microscopy

Chromatin

Cardiac hypertrophy

## ABSTRACT

Despite the extensive knowledge of the functional unit of chromatin—the nucleosome—for which structural information exists at the atomic level, little is known about the endogenous structure of eukaryotic genomes. Chromosomal capture techniques and genome-wide chromatin immunoprecipitation and next generation sequencing have provided complementary insight into global features of chromatin structure, but these methods do not directly measure structural features of the genome *in situ*. This lack of insight is particularly troublesome in terminally differentiated cells which must reorganize their genomes for large scale gene expression changes in the absence of cell division. For example, cardiomyocytes, which are fully committed and reside in interphase, are capable of massive gene expression changes in response to physiological stimuli, but the global changes in chromatin structure that enable such transcriptional changes are unknown. The present study addressed this problem utilizing super-resolution stimulated emission depletion (STED) microscopy to directly measure chromatin features in mammalian cells. We demonstrate that immunolabeling of histone H3 coupled with STED imaging reveals chromatin domains on a scale of 40–70 nm, several folds better than the resolution of conventional confocal microscopy. An analytical workflow is established to detect changes in chromatin structure following acute stimuli and used to investigate rearrangements in cardiomyocyte genomes following agonists that induce cellular hypertrophy. This approach is readily adaptable to investigation of other nuclear features using a similar antibody-based labeling technique and enables direct measurements of chromatin domain changes in response to physiological stimuli.

© 2012 Elsevier Ltd. All rights reserved.

## 1. Introduction

What the interphase genome looks like *in vivo* is unknown. Advances in sequencing over the last decade have provided new insight into sequence variants [1,2] and their expression [3]; yet how the genome is organized in three dimensions, apart from the well-described machinations of mitosis, is only beginning to be understood [4,5]. Cardiac myocytes reside primarily in interphase but are capable of large-scale changes in gene expression. Transcription factors, histone modifying enzymes and RNA polymerase complexes play a central role in the process of gene expression—however, an equally important and less explored factor is endogenous chromatin structure.

To be transcribed, a gene's local environment must be accessible for protein binding. A critical question remains unknown: how is the genome appropriately poised to have the right genes on and off under “basal” conditions, and what are the mechanisms that globally reorganize chromatin following a stimulus (e.g. during disease)?

The packaging of DNA in the nucleus occurs on the basis of the following structural hierarchy: a segment (~147 bp) of DNA wraps around a protein complex containing two copies each of four core histones (H2A, H2B, H3 and H4), constituting a nucleosome; this octameric protein complex in turn forms higher ordered structures of less well-defined architecture through interactions with linker histones (like H1) and other chromatin structural proteins (e.g. high mobility group proteins). These higher order chromatin regions determine the overall shape and presentation of each region of the genome. Histones are beset by a battery of enzymes that influence nucleosome integrity and positioning through post-translational modification (PTM). The most extensively characterized tri-methylation modifications of histone H3 have opposing effects: lysine 9 tri-methylation causes heterochromatin formation and silences genes [6,7], whereas lysine 4

\* Correspondence to: T.M. Vondriska, Department of Anesthesiology, David Geffen School of Medicine, University of California, Los Angeles, USA. Tel.: +1 310 206 4188.

\*\* Correspondence to: L.A. Bentolila, California NanoSystems Institute, University of California, Los Angeles 570 Westwood Plaza Building 114 Los Angeles CA 90095-7277, USA. Tel.: +1 310 983 1076; fax: +1 310 267 4918.

E-mail addresses: [lbento@chem.ucla.edu](mailto:lbento@chem.ucla.edu) (L.A. Bentolila), [tvondriska@mednet.ucla.edu](mailto:tvondriska@mednet.ucla.edu) (T.M. Vondriska).

tri-methylation contributes to euchromatin formation and activates genes [8,9].

Recent advances in fluorescence imaging methods have overcome the fundamental limitation of the diffraction resolution barrier imposed on optical microscopes that use focused light [10]. In STED microscopy [11], a pulsed excitation beam is overlapped with a second doughnut-shaped pulsed beam (the “STED” beam) whose role is to limit the fluorescence emission of the fluorescent molecules solely to the ones located within the center of the “doughnut hole” (5, 24). Fluorescent molecules located on the overlapping rim regions of both the excitation and red-shifted STED beams are depleted without formation of detectable photons, thus annihilating fluorescence emission. As a result, the emission is confined to an area that is much smaller than that normally covered by a conventional diffraction-limited excitation spot. Raster-scanning of the two interlocked beams across the sample allows for the acquisition of fluorescent images below the diffraction limit which is defined as roughly half the wavelength of the excitation light beam (that is >200 nm in the visible spectrum) to possibly down to 6 nm in the imaging plane [12]. This technique has been exploited in several biological settings including neurotransmitter exocytosis [13] and to examine protein localization in mitochondria [14].

The objective of the present study was to utilize STED microscopy to visualize chromatin structure in cardiac cells and to develop a framework for characterizing rearrangement in this structure following physiological stimuli. Because of the super-resolution abilities of STED, such an approach has the ability, in principle, to measure individual chromatin domains on the scale of tens of nanometers, which would significantly improve our understanding of endogenous genomic structure, which currently lacks intermediate structural details *in situ* between the nucleosome and the entire chromosome level.

## 2. Materials and methods

Neonatal rat ventricular myocytes (NRVMs) were obtained by enzymatic dissociation from 1 day old litters and plated in DMEM media (Invitrogen, #11965) containing 1% penicillin, 1% streptomycin, 1% insulin–transferrin–sodium selenite supplement and 10% fetal bovine serum for the first 24 h after which the cells are cultured in serum- and antibiotic-free media [15–17]. This protocol has been approved by the UCLA Chancellor’s Animal Research Committee. For cell size analysis NRVMs were fixed with 4% paraformaldehyde, incubated with  $\alpha$ -actinin antibody (Sigma, A7811, mouse) and imaged on a Nikon Eclipse TE2000-U. Isoproterenol (ISO) [18] was added to a concentration of 1  $\mu$ M for 24 or 48 h to induce hypertrophy.

We adapted published protocols [13,30] for immunohistochemistry of NRVMs for STED microscopy analysis. Glass coverslips in a 24-well plate are coated with poly-L-lysine and incubated for 30 min at room temperature (RT), after which poly-L-lysine is removed and coverslips are allowed to dry. Freshly isolated NRVMs are added in media to coverslips and incubated overnight at 37 °C in 5% CO<sub>2</sub>. The media is then removed, cells are washed three times with cold PBS, rinsed once with 4% paraformaldehyde and incubated with fresh 4% paraformaldehyde for 20 min at RT. After three more washes with cold PBS, cells are incubated with 0.3% Triton X-100 in PBS for 20 min, washed again, and blocked with 5% BSA in PBS for 1 h at RT. Primary antibodies histone H3 1:1000 dilution (Abcam Ab1791; rabbit), RNA POLII 1:500 dilution (Active Motif 102662; mouse) and H3K4Me3 1:500 dilution (Abcam Ab8580; rabbit) are incubated in PBS containing 2.5% BSA (or normal 1.0% donkey/goat serum with 0.2% Triton X-100 in PBS) overnight at 4 °C. After three washes in PBS-T, secondary antibody is added (ATTO-647N goat anti-rabbit dye 1:1000 dilution from Active Motif #15048, ATTO-647N goat anti-mouse dye 1:1000 dilution from Active Motif #15038, Alexa Fluor 488 goat anti-rabbit dye 1:1000 dilution from Invitrogen #A11008, Alexa Fluor 568 goat anti-mouse dye 1:1000

dilution from Invitrogen #A11004) in PBS and incubated for 1 h at RT in darkness. The cells were washed three more times in PBS-T and dehydrated with successive concentrations of (10%, 25%, 50%, 2 $\times$  97%) thiodiethanol (TDE) for 5 min each.

Super-resolution images were obtained using a Leica TCS SP5 STED confocal system (Leica Microsystems, Wetzlar, Germany) equipped with an oil immersion objective (HCX PL APO CS 100 $\times$ /1.40NA STED). A 640 nm pulsed diode laser (PicoQuant, Germany) was used for excitation. The pulses for STED depletion were delivered using a tunable ultrafast Ti:Sapphire laser (Mai Tai® Broadband, Spectra-Physics, CA) emitting at a wavelength of 750 nm. Red fluorescence emitted from the ATTO 647N-labeled antibody was collected through a Semrock BrightLine® 685/40-25 nm band pass filter (FF01-685/40-25, Semrock, Rochester, NY) in front of an avalanche photodiode (APD, PerkinElmer, Waltham, MA). Optical sectioning was achieved by using a detection pinhole set to 1 Airy. Scanning was performed at a line frequency of 200 Hz with an image format of 1024 $\times$ 1024 pixels. Each frame was averaged 4 times. Pixel size was kept under 16 nm $\times$ 16 nm by applying a 9.5 $\times$  to 11.5 $\times$  digital zoom. For comparison, all imaging parameters were kept identical between the confocal and STED image counterpart except for increasing the APD gain up to 7% when recording the STED image to compensate for the slight loss of signal in STED microscopy resulting from the shrinking of the effective excitation spot. It should be noted that the small pixel size resulted in oversampling of the confocal images which could cause some photobleaching. Images were processed using Matlab R2009a. Briefly, STED image files were converted to grayscale images using the function ‘rgb2gray’ in the Image Processing Toolbox, then converted to contour plot using the function ‘contour’ with default parameters.

## 3. Results

To develop a method for direct visualization of chromatin structure *in situ*, we utilized state-of-the-art STED microscopy to image nuclei from cardiac and other cell types. As a component of all nucleosomes, histone H3 is an attractive candidate to label the chromatin backbone. Using conventional confocal microscopy, some features of chromatin structure are apparent when imaging histone H3-labeled cells, but these become resolved strikingly better when combined with depletion in STED mode (Fig. 1). As shown in the overlay images (Fig. 1, bottom panel), STED reveals discrete foci of chromatin and additional anatomical features not discernable with conventional microscopy; in other words, it is not possible to computationally derive the information contained in a STED image from the traditional confocal image, as the former is not simply a better focused version of the latter. The patterns we observed in NRVM nuclei were very reproducible between multiple cells and preparations (Supplemental Fig. 1) and the global features described by histone H3 labeling were similar across different cell types, including HeLa (Fig. 2B), HEK293 (Fig. 2C) and neurons (Fig. 3C). Labeling of nucleosomes with a separate primary antibody (against trimethylated lysine 4 on histone H3) demonstrated the same pattern (Supplemental Fig. 3), ruling out antibody-specific effects, and omission of the primary antibody or peptide disruption both obliterated the labeling pattern (Supplemental Figs. 4A and B), demonstrating the specificity of the labeling.

To estimate the resolution of the method, we performed several line scans in typical STED images of NRVM chromatin. As shown in Fig. 2A and Supplemental Figs. 1B and C, we reproducibly obtain resolution of 40–70 nm in biological specimens, distinguishing features <200 nm apart—over three times better than conventional microscopes. We next considered the possibility that the chromatin features revealed by STED were a unique plane of the nucleus due to limited antibody accessibility and not representative of the global chromatin architecture. To rule out this possibility, we performed

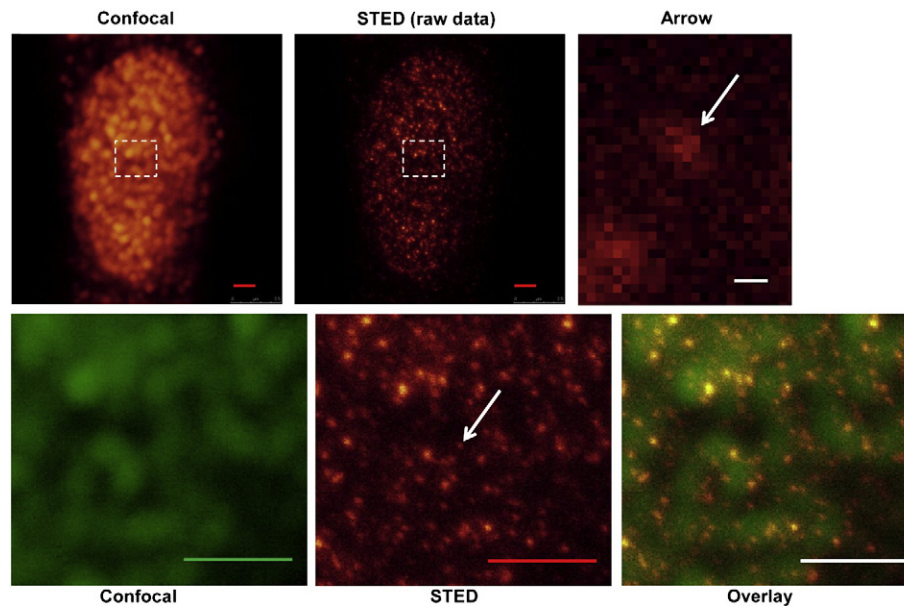


**Fig. 1.** Super-resolution visualization of cardiac chromatin via STED microscopy. Top panels, left to right: confocal imaging of histone H3; STED image of the same nucleus; and zoom image of region indicated by arrow in bottom middle panel. Individual pixels in the STED images are 14–16 nm. Bottom panels, higher magnification images of boxed area in top panels: confocal (false colored green); STED; and overlay. Bar is 1  $\mu\text{m}$  in all images except top right, where it is 50 nm.

serial imaging in the z plane, demonstrating that in fact the antibodies effectively label throughout the nucleus (Fig. 2D) and thus serve as a reliable tracer for the chromatin fiber *in situ*. The appearance of chromatin was indistinguishable between individual nuclei in bi-nucleated NRVMs (Supplemental Fig. 5), which constituted 1–2% of the cells in our populations.

To investigate the relationship of the chromatin backbone to specific functions of the nucleus, we examined regions of mRNA transcription by labeling for RNA polymerase II (RNA POLII). Surprisingly, RNA POLII staining was strongest in the nuclear periphery in NRVMs (Fig. 3A), with various areas of localized intensity decorating the sub-nuclear membrane space. Unlike histone H3, RNA POLII staining did not exhibit the discrete puncta associated with the chromatin backbone, as evidenced by the fact that when RNA POLII is imaged in the STED channel, the individual areas of localized intensity remain but discrete puncta like those seen for histone H3 are not observed (Fig. 3B). These patterns were very reproducible (Supplemental Fig. 2A) and appeared to be unique for cardiac cells, as primary neurons displayed diffuse RNA POLII labeling (Fig. 3C and Supplemental Figs. 2B and C) despite the similar appearance of histone H3 in these cells. The pattern of RNA POLII staining in NRVMs was unaffected by ISO in this study.

Lastly, we sought to determine whether this method of chromatin imaging could be used to discover heretofore unrecognized global rearrangement in chromatin following a biologically relevant stimulus *in situ*. NRVMs were treated with vehicle or the hypertrophic agonist isoproterenol (ISO, 1  $\mu\text{M}$ ) and imaged 24 or 48 h later. We performed image intensity analysis to recover 3D data in a 2D image, generating intensity contour plots (Fig. 4A) from vehicle- or ISO-treated cells (which exhibit hypertrophic growth, Fig. 4B). Global differences in the chromatin pattern were immediately apparent from these analyses. To quantify this effect, we examined the intensity of pixels in images from vehicle-treated cells or those at 24 or 48 h after ISO ( $n > 25$  cells/group) and plotted this data as a fraction of the nucleus. As shown in the representative images in Fig. 4A and as a histogram for all cells analyzed in Fig. 4C (red bar), there was a substantial increase in zero intensity regions of the image following hypertrophic stimulation (*i.e.* more of the pixels in the nuclear field had no signal for histone H3). This trend is also apparent when the cumulative distribution of pixel intensities is plotted for the

individual treatment groups (Fig. 4D). The purpose of the contour plot is to render in two dimensions the differential intensity obtained from the imaging of a three dimensional specimen, akin to how topographical maps indicate the earth's terrain. In this way, changes in local intensity are represented in a manner independent of overall intensity, the latter varying between images. In the case of histone H3 labeling in this study, the contour plot is a measure of chromatin crowding, or density; the total signal in each raw image is very similar, however, the relative crowding is very different. In the vehicle-treated NRVM (Fig. 4A, top), there is a substantial amount of moderate intensity chromatin, indicated in the contour plot as dark blue, with a small amount of high intensity chromatin, indicated as red in the contour plot. ISO treatment changes this pattern in three ways as revealed by the contour plot: first, the amount of very low intensity chromatin (white in the contour plot; note: this region is black in the raw image, indicative of no signal, and the red bar in the histogram in panel C) is significantly increased; second, and related to the first observation, the moderate intensity chromatin (dark blue in contour plot) is diminished; and third, the very high intensity foci (orange and red in contour plot) are increased. The collective interpretation of these changes is that ISO induces some regions of chromatin to become more compact (the very intense foci in the raw image and the high intensity chromatin in the contour plot) while simultaneously freeing up large portions of the nucleus for gene expression, including protein recruitment—as represented by the zero intensity white areas in the contour plot.

#### 4. Discussion

During mitosis, the shape of the chromosomes is well established—as are the highly orchestrated structural events during cytokinesis. The 3D structure of the non-mitotic genome, however, is poorly understood. The packing task of the nucleus is daunting: two copies of the ~3 billion base pair genome must be collapsed into the nuclear space; accommodation must also be made for RNA and protein (we have measured > 1000 proteins in the cardiac nucleus [19], including > 300 bound to chromatin [19]), while still maintaining conformational flexibility to enable large, rapid changes in gene expression. New insights into genomic structure provided by techniques like chromosomal conformation capture [4,5] have demonstrated a non-random structure

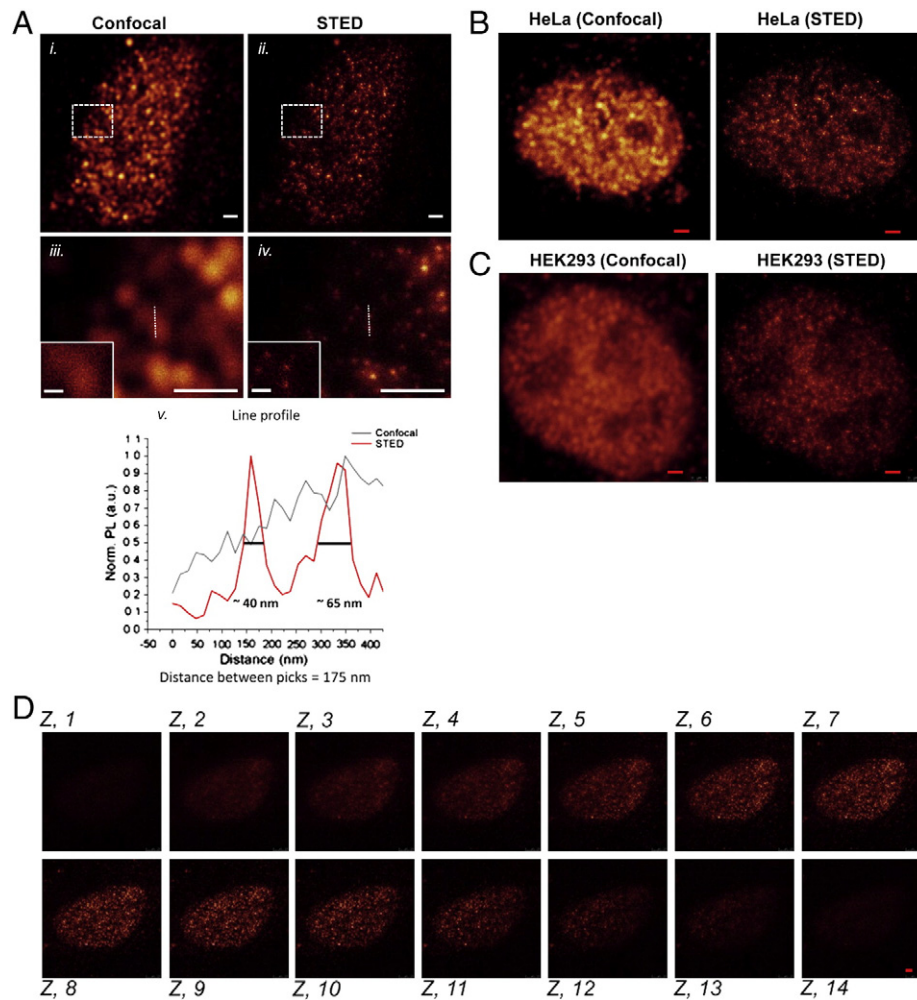


**Fig. 2.** Resolution of STED. Panel A, line scans demonstrate vastly superior resolution obtained with STED as compared to conventional confocal imaging of the same field. Panels iii and iv are zoom images of i and ii, respectively; panel v shows the line scan profile which displays resolution of two distinct foci (red line; distance between STED peaks is 175 nm) in STED image that are not resolved in the conventional confocal (gray line) data. Inset in panels iii and iv shows the area of analysis at higher magnification. Typical resolution, measured at full-width half-maximum (FWHM), with this method is 40–70 nm (see also Supplemental Figs. 1B and C). Using this method, nuclei from HeLa (panel B) and HEK293 cells (panel C) were similarly labeled with histone H3 antibodies and the same field visualized *via* conventional confocal or STED microscopy. Panel D, serial z stack STED images of histone H3 in myocytes (taken at 0.5  $\mu\text{m}$  intervals along the z axis) demonstrate architecture of chromatin throughout the *in situ* nucleus. Bar is 1  $\mu\text{m}$  in all images except insets where it is 0.2  $\mu\text{m}$ .

of the genome in an interphase nucleus, and suggest that coordinated packaging of chromosomal territories is a critical task to enable global gene expression programs in eukaryotes. In these investigations, cross-linking of DNA regions near each other in three dimensions, followed by DNA sequencing and computational analyses, allows for determination of *in vivo* chromosomal territories and the determination of the fractal properties of the interphase genome. The present study was designed to develop a method to visualize, directly, the chromatin backbone by super-resolution microscopy to provide structural information to complement existing sequencing/computational data. We demonstrate reproducible and quantitative mapping of chromatin domains at a resolution several fold better than that obtained with conventional confocal microscopy (on the scale of 40–70 nm), discerning global features of genome packing never before reported in cardiac nuclei. Our method is comparable to similar approaches with dSTORM in eukaryotes [20] or bacteria [21] and DNA-based fluorescence *in situ* hybridization (FISH) techniques [22] (both of which image on the scale of ~100 nm) but has the advantage of not requiring genetic tagging methods, making it directly applicable to any biological specimen. Such methods have great potential to advance our understanding of endogenous genome behavior in living cells [23].

We were intrigued by the peripheral localization of RNA POLII in myocytes (Figs. 3A,B, and Supplemental Fig. 2A), which was not observed in the other cells we tested (Fig. 3C and Supplemental Fig. 2B). In support of the uniqueness of this observation, a recent study [24] examining the chromatin architecture in the rods of nocturnal versus diurnal animals reported a fundamental difference in the nuclear features in these distinct animals. Specifically, diurnal rods exhibit what the authors refer to as a “conventional” chromatin architecture, which, in brief, localizes heterochromatin elements to the nuclear periphery and areas of active transcription to the center of the nucleus. This conventional architecture, so called because most mammalian cell types exhibit it (although the authors did not examine cardiac myocytes), is contrasted with an “inverted” architecture, which, as the name implies, sees the heterochromatin restricted to the nuclear interior with the euchromatin in the periphery. Although this study did not measure RNA POLII localization, this protein can reasonably be considered to be a marker of euchromatin. The present observation is an important contribution to this model in that it suggests cells other than the nocturnal rod may exhibit the inverted chromatin architecture.

The region of the nucleus occupied by the genome was calculated by setting a signal intensity threshold in the confocal image which

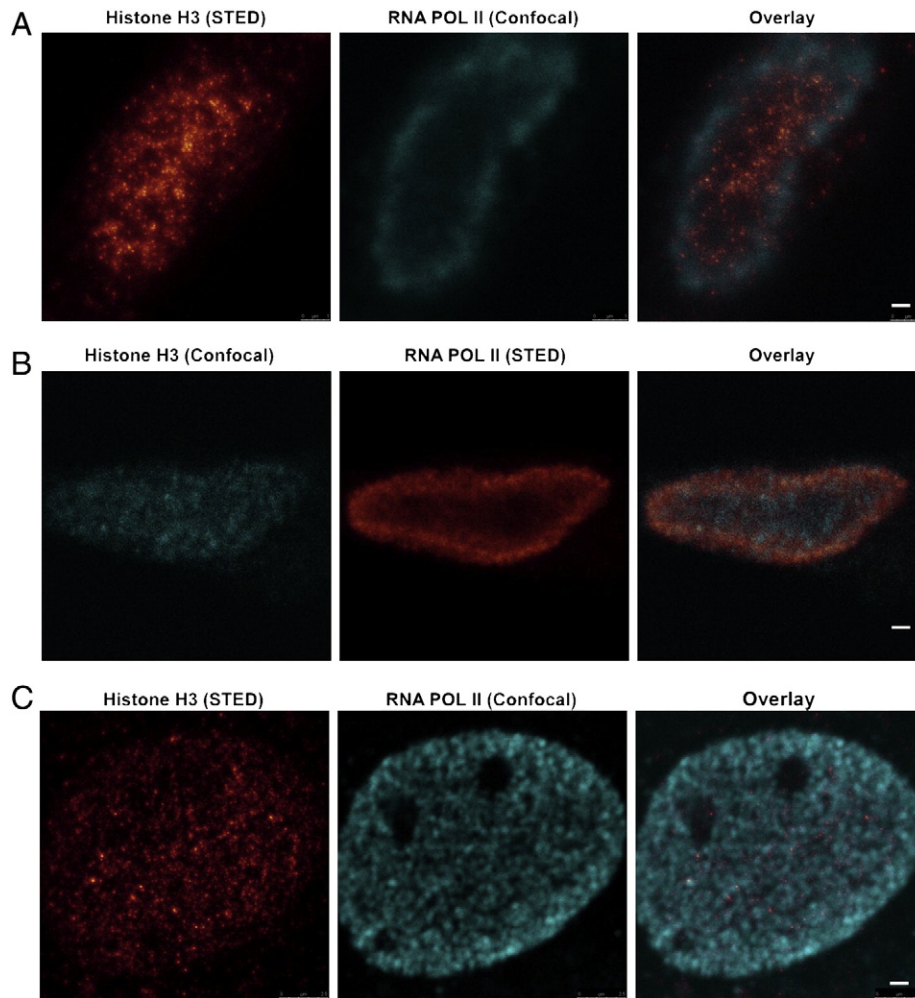


**Fig. 3.** Localization of RNA POLII and its features as revealed by STED. Panel A, NRVMs were labeled with histone H3 and RNA POLII, simultaneously visualized *via* STED (red) or conventional confocal (cyan), respectively. Panel B, same as previous panel with the RNA POLII visualized in STED channel (red) and histone H3 in conventional confocal (cyan). RNA POLII displayed diffuse staining throughout the nucleus, with concentrations in the nuclear periphery. This pattern was unique to NRVMs, as neurons displayed a more homogenous distribution of RNA POLII despite a similar global histone H3 pattern (panel C). Bar is 1  $\mu\text{m}$  in all images.

was used to record protein signal in a digital manner. This measurement was further enhanced by examining relative intensities of signal to generate the contour plot analyses and determine the density of packing in different regions and under different conditions (here, before and after the hypertrophic agonist isoproterenol, Fig. 4). These analyses reveal that the percentage of the nucleus occupied by the histone H3-labeled chromatin shifts from 93% under basal conditions to 73–76% following isoproterenol (Figs. 4C and D). We interpret this observation as indicative of more open areas in the nucleus, possibly allowing space for transcriptional activities, although this conjecture requires experimental confirmation. In principle, given the complete labeling of the nucleus obtained with the immunostaining method used herein (Fig. 2D), this method allows the chromatin backbone to be traced in a given z plane, and rearrangements in this backbone measured following various stimuli (Fig. 5). Because STED microscopy does not improve resolution in the z dimension, and owing to the high complexity of information in the 2D STED images, such tracing of chromatin fibers will not be a straightforward exercise and will require specialized image analysis tools more sophisticated than those presented herein.

The effect of ISO on chromatin structure was examined in the present study, although it will be critical to evaluate the role of other hypertrophic agonists and known chromatin remodelers in future work. It has been recognized for some time that different chromatin remodeling enzymes, HDACs and HATs in particular, may

differentially regulate the hypertrophic gene expression profiles in response to various stimuli [25]. Recent work with chromatin structural proteins suggests that these molecules may also be differentially involved in chromatin structure during normal and diseased cardiac states: the high mobility group B (HMGB) family of proteins exhibits distinct expression patterns following stimulation of NRVMs with ISO, endothelin (ET) or phenylephrine (PHE). ISO and PHE increase nuclear abundance of HMGB1 and HMGB2, whereas ET increases HMGB2 but decreases HMGB1. Furthermore, loss-of-function studies indicate that HMGB2 but not HMGB1 suppresses an endogenous gene expression profile associated with hypertrophy [17]. These findings suggest that, similar to what is seen in the metabolic and signaling responses, chromatin remodeling in the wake of distinct hypertrophic agonists is variable, with the potential common observation being a shift toward more active chromatin states.

We do not detect any changes in K4Me3 modified histone H3 following agonist treatment as detected by STED (Supplemental Fig. 4 and data not shown), and speculate that such changes may be too nuanced to be detected even with this super-resolution technique. To be more specific, it is probably that there is a rearrangement of modifications from one set of nucleosomes to another (rather than a total change in abundance), although this is speculation and would have to be resolved by techniques that discriminate between individual nucleosomes, like genome-wide chromatin immunoprecipitation and DNA sequencing (ChIP-seq), which microscopy cannot do at

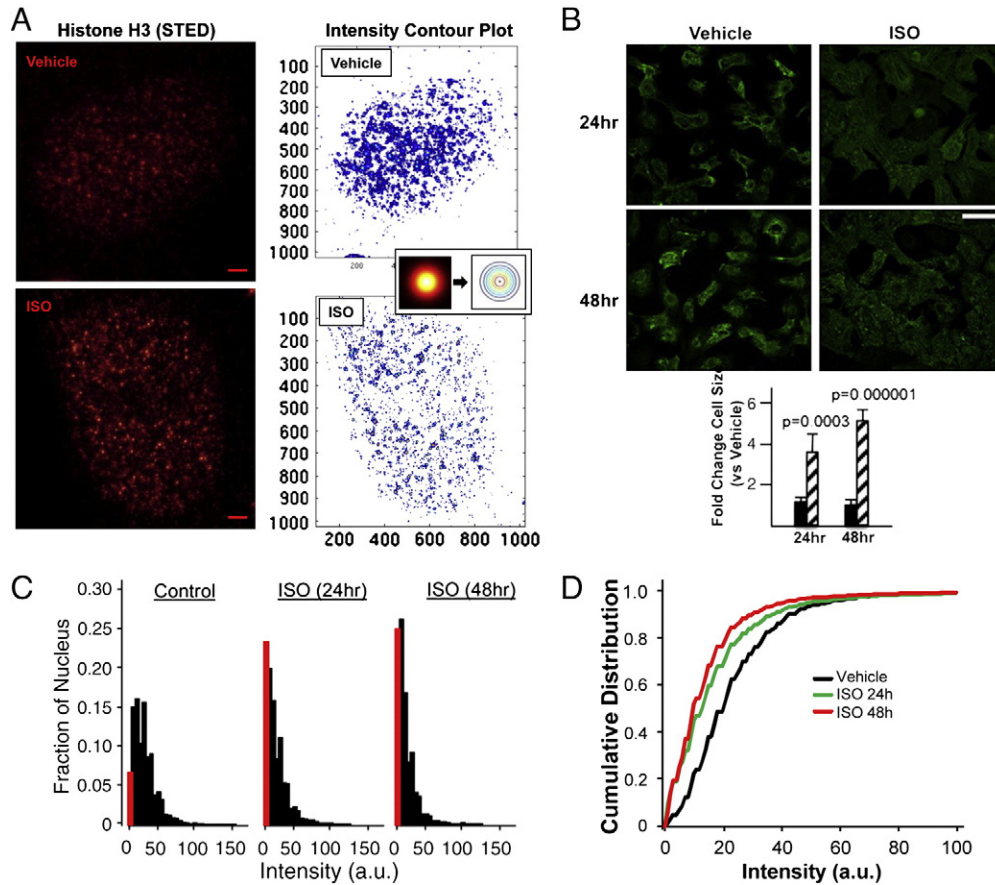


**Fig. 4.** Global chromatin changes after hypertrophic agonists detected by STED microscopy. NRVMs were treated with isoproterenol (ISO, 1  $\mu$ M) or vehicle and examined 24 or 48 h later. Panel A, STED images of histone H3 labeling were acquired in each condition and intensity contour analysis performed, examples of which are shown in this panel. Bar is 1  $\mu$ m. Panel B, ISO induces hypertrophy in NRVMs, as described [18]. Cells are labeled with alpha-actinin and visualized by confocal microscopy at either 24 (top panels) or 48 (bottom panels) hours after ISO. Bar is 50  $\mu$ m. Histogram displays quantitative data on cell size changes (SEM displayed). Panel C, STED images from histone H3 labeled vehicle or ISO-treated cells (24 or 48 h) were examined as in panel A and the number of pixels (*i.e.* the fraction of the nucleus, y-axis) at a given intensity (x-axis, in arbitrary units) tabulated for the region of the cell constituting the nucleus ( $n > 25$  cells/group). Note that the control cells have a small fraction of low intensity staining (red bar) that increases after ISO treatment. Panel D, shows the same data (intensity in same arbitrary units) as panel C, plotted as cumulative distribution of pixel intensity (intensities greater than 100 a.u. are included in the distribution but not shown as the lines become superimposed at very high intensities due to low frequency).

this time. Such ChIP-seq studies have been conducted in rat hearts during failure and indicate global reorganization of hetero- and eu-chromatin marks is pervasive in this disease [26]. We have observed altered histone post-translational modifications in response to alterations in chromosomal structural protein abundance [17], as well as in response to physiological hypertrophic stressors like pressure overload (unpublished observations).

Depending on the cell type, the mammalian nucleus can vary in diameter from  $<5$  to  $>10$   $\mu$ m, which, if assumed to be spherical, would give volumes ranging from  $<65.5$  to  $>524$   $\mu$ m<sup>3</sup>. In this study, most NRVM nuclei tended to be non-spherical, egg-shaped ellipsoids, with the long axis ranging from 8.25 to 11.6  $\mu$ m and the short axis from 5.0 to 7.9  $\mu$ m; these dimensions would lead to nuclear volumes of 118–369  $\mu$ m<sup>3</sup>.

*What portion of the nucleus is occupied by the genome?* To address this question from a structural standpoint, the genome is assumed to have two constitutive components: DNA and core nucleosomal histones (two copies each of H2A, H2B, H3 and H4). Based on structural information available for these two components [27,28], combined with their respective stoichiometry in the nucleus, we estimate the portion of the nucleus occupied by the genome to be  $\sim 4\%$  (in non-myocytes, this could range as low as 2% in the larger nuclei or as high as 15% in smaller ones). Of course the actual volume occupied can only be greater than this, because the foregoing calculations assume perfect packing of the genome, with no gaps, which is biologically untenable. Thus, while the genome is clearly capable of being

packaged within the nucleus, the minimal volume occupied by this DNA–protein complex is a sizable portion of the physical space within this organelle.

Recent studies using genome-wide chromosomal capture techniques have begun to reveal the features of endogenous interphase genomes [4,5], albeit in dividing cells. These studies reinforce the concept of chromosomal territories, in which non-random association of chromosomal regions *in vivo* reproducibly creates chromatin environments made up of the same loci. These areas presumably have critical importance for gene expression profiles in given cell types. Our findings regarding the peripheral localization of RNA POLII in neonatal myocytes (Fig. 3A and Supplemental Fig. 2A) challenge the contention that most cells position areas of active transcription in the center of the nucleus and support the localized actions of RNA POLII for mRNA transcription in the focal areas of intense staining around the nuclear membrane in NRVMs. What remains unclear is whether the patterns of chromatin structure, and the changes commensurate with agonist treatment, faithfully recapitulate the occurrences in the intact heart muscle in conditions of pathologic hypertrophy. A strength of the methodology as described herein is that it is in principle applicable to any biological specimen interrogated by conventional confocal microscopy, including intact heart muscle; such studies would reveal whether isolated cell alters chromatin structure directly and what features of chromatin structure are exhibited by the non-myocyte cells in the heart. Future studies combining this method with DNA FISH, to track specific chromosomes or genomic

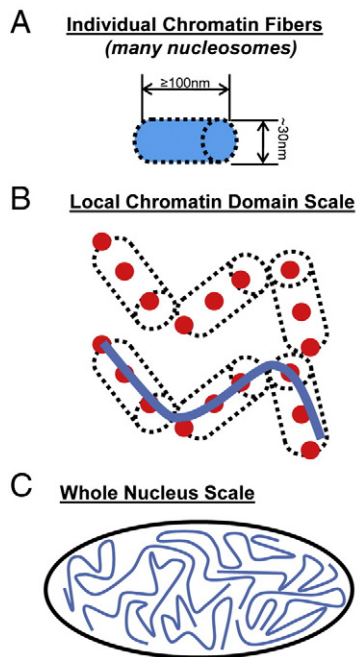


**Fig. 5.** Interpretation of STED images and potential for *in situ* chromatin measurements. Panel A, measured dimensions of chromatin fibers *in vitro*, which contain dozens of individual nucleosomes [29]. Panel B, the resolution of the STED microscope allows labeling of endogenous chromatin fibers (hashed cylinders; red dots are foci in STED images) which can then be traced to discern local structure (blue line). Panel C, when applied to the entire nucleus, this technique in principle allows for determination of *in situ* chromatin architecture in cardiac and other cells.

loci, will provide a sequence-specific frame of reference for the global rearrangements in the chromatin backbone determined by nucleosome-based immunocytochemistry.

Supplementary related to this article can be found online at <http://dx.doi.org/10.1016/j.yjmcc.2012.07.009>.

#### Author contributions

SM-J and LAB conducted experiments; TMV and SF conceived of the study; SM-J, LAB, TMV and HC analyzed the data; LAB and ES provided equipment and expertise; TMV wrote the paper; all authors reviewed the final manuscript.

#### Grants

This study was supported by R01 HL105699 (TMV), R01 HL088640 (ES) and the Laubisch Endowment at UCLA (TMV). HC is the recipient of an American Heart Association Predoctoral Fellowship and SF of a K99 award from the NHLBI. The CNSI Advanced Light Microscopy/Spectroscopy Laboratory is supported in part by funding from an NSF Major Research Instrumentation Grant (CHE-0722519).

#### Disclosures

None.

#### Acknowledgments

The authors thank Drs. Jeff Abramson and Vincent Chaptal for helpful discussions, Dr. Baljit Khakh for primary rat neurons and Dr. Robb MacLellan for neonatal rat ventricular myocytes. STED confocal laser scanning microscopy was performed at the California NanoSystems Institute (CNSI) Advanced Light Microscopy/Spectroscopy Laboratory at UCLA.

#### References

- Alexander RP, Fang G, Rozowsky J, Snyder M, Gerstein MB. Annotating non-coding regions of the genome. *Nat Rev Genet* 2010;11:559–71.
- Raney BJ, Cline MS, Rosenbloom KR, Dreszer TR, Learned K, Barber GP, et al. ENCODE whole-genome data in the UCSC genome browser (2011 update). *Nucleic Acids Res* 2011;39:D871–5.
- Wang Z, Gerstein M, Snyder M. RNA-Seq: a revolutionary tool for transcriptomics. *Nat Rev Genet* 2009;10:57–63.
- Lieberman-Aiden E, van Berkum NL, Williams L, Imakaev M, Ragoczy T, Telling A, et al. Comprehensive mapping of long-range interactions reveals folding principles of the human genome. *Science* 2009;326:289–93.
- van Steensel B, Dekker J. Genomics tools for unraveling chromosome architecture. *Nat Biotechnol* 2010;28:1089–95.
- Bannister AJ, Zegerman P, Partridge JF, Miska EA, Thomas JO, Allshire RC, et al. Selective recognition of methylated lysine 9 on histone H3 by the HP1 chromatin domain. *Nature* 2001;410:120–4.
- Lachner M, O'Carroll D, Rea S, Mechtler K, Jenuwein T. Methylation of histone H3 lysine 9 creates a binding site for HP1 proteins. *Nature* 2001;410:116–20.
- Nishioka K, Chuikov S, Sarma K, Erdjument-Bromage H, Allis CD, Tempst P, et al. Set9, a novel histone H3 methyltransferase that facilitates transcription by precluding histone tail modifications required for heterochromatin formation. *Genes Dev* 2002;16:479–89.
- Strahl BD, Ohba R, Cook RG, Allis CD. Methylation of histone H3 at lysine 4 is highly conserved and correlates with transcriptionally active nuclei in *Tetrahymena*. *Proc Natl Acad Sci U S A* 1999;96:14967–72.
- Hell SW. Far-field optical nanoscopy. *Science* 2007;316:1153–8.
- Willig KI, Kellner RR, Medda R, Hein B, Jakobs S, Hell SW. Nanoscale resolution in GFP-based microscopy. *Nat Methods* 2006;3:721–3.
- Rittweger E, Han K, Irvine S, Eggeling C, Hell SW. STED microscopy reveals crystal colour centres with nanometric resolution. *Nat Photonics* 2009;3:144–7.
- Willig KI, Rizzoli SO, Westphal V, Jahn R, Hell SW. STED microscopy reveals that synaptotagmin remains clustered after synaptic vesicle exocytosis. *Nature* 2006;440:935–9.
- Singh H, Lu R, Rodriguez PF, Wu Y, Bopassa JC, Stefani E, et al. Visualization and quantification of cardiac mitochondrial protein clusters with STED microscopy. *Mitochondrion*. 2011.
- Engel FB, Schebesta M, Duong MT, Lu G, Ren S, Madwed JB, et al. p38 MAP kinase inhibition enables proliferation of adult mammalian cardiomyocytes. *Genes Dev* 2005;19:1175–87.
- MacLellan WR, Garcia A, Oh H, Frenkel P, Jordan MC, Roos KP, et al. Overlapping roles of pocket proteins in the myocardium are unmasked by germ line deletion of p130 plus heart-specific deletion of Rb. *Mol Cell Biol* 2005;25:2486–97.
- Franklin S, Chen H, Mitchell-Jordan SA, Ren S, Wang Y, Vondriska TM. Quantitative analysis of chromatin proteome reveals remodeling principles and identifies HMGB2 as a regulator of hypertrophic growth. *Mol Cell Proteomics*. 2012.
- Iaccarino G, Dolber PC, Lefkowitz RJ, Koch WJ. Beta-adrenergic receptor kinase-1 levels in catecholamine-induced myocardial hypertrophy: regulation by beta- but not alpha1-adrenergic stimulation. *Hypertension* 1999;33:396–401.
- Franklin S, Zhang MJ, Chen H, Paulsson AK, Mitchell-Jordan SA, Li Y, et al. Specialized compartments of cardiac nuclei exhibit distinct proteomic anatomy. *Mol Cell Proteomics* 2011;10:703.
- Wombacher R, Heidebreder M, van de Linde S, Sheetz MP, Heilemann M, Cornish VW, et al. Live-cell super-resolution imaging with trimethoprim conjugates. *Nat Methods* 2010;7:717–9.
- Wang W, Li GW, Chen C, Xie XS, Zhuang X. Chromosome organization by a nucleoid-associated protein in live bacteria. *Science* 2011;333:1445–9.
- Bystricky K, Heun P, Gehlen L, Langowski J, Gasser SM. Long-range compaction and flexibility of interphase chromatin in budding yeast analyzed by high-resolution imaging techniques. *Proc Natl Acad Sci U S A* 2004;101:16495–500.
- Horowitz-Scherer RA, Woodcock CL. Organization of interphase chromatin. *Chromosoma* 2006;115:1–14.
- Solovei I, Kreysing M, Lanctot C, Kosem S, Peichl L, Cremer T, et al. Nuclear architecture of rod photoreceptor cells adapts to vision in mammalian evolution. *Cell* 2009;137:356–68.
- McKinsey TA, Olson EN. Dual roles of histone deacetylases in the control of cardiac growth. *Novartis Found Symp*. 2004;259:132–41; discussion 41–5, 63–9.
- Kaneda R, Takada S, Yamashita Y, Choi YL, Nonaka-Sarukawa M, Soda M, et al. Genome-wide histone methylation profile for heart failure. *Genes Cells* 2009;14:69–77.
- Mandelkern M, Elias JG, Eden D, Crothers DM. The dimensions of DNA in solution. *J Mol Biol* 1981;152:153–61.
- Wong H, Victor JM, Mozziconacci J. An all-atom model of the chromatin fiber containing linker histones reveals a versatile structure tuned by the nucleosomal repeat length. *PLoS One* 2007;2:e877.
- Tremethick DJ. Higher-order structures of chromatin: the elusive 30 nm fiber. *Cell* 2007;128:651–4.
- Farahani JN, Schibler MJ, Bentolila LA. Stimulated emission depletion (STED) microscopy: from theory to practice. In: Mendez-Vilas A, Diaz J, editors. *Microscopy science, technology, applications and education*, vol. II, No 4. Badajoz, Spain: Formatec Research Center Publishing; 2010. p. 1539–47.